Supporting Information

Interfacial energy band engineered $CsPbBr_3$/NiFe-LDH heterostructure catalyst with tunable visible light driven photocatalytic CO_2 reduction capability

Haoyue Sun[a], Rui Tang[a], Xingmo Zhang[a, b], Shuzhen Zhang[a], Wenjie Yang[a], Lizhuo Wang[a], Weibin Liang[a], Fengwang Li[a], Rongkun Zheng[b] and Jun Huang*[a]*

[a] School of Chemical and Biomolecular Engineering, Sydney Nano Institute, The University of Sydney, New South Wales 2006, Australia

[b] School of Physics, Sydney Nano Institute, The University of Sydney, New South Wales, 2006, Australia

* Corresponding authors

Dr. Rui Tang, E-mail: rui.tang2@sydney.edu.au

Prof. Jun Huang, E-mail: jun.huang@sydney.edu.au

1. Experimental

1.2 Chemical and reagents

Iron(II) sulfate heptahydrate ($FeSO4 \cdot 7H_2O$, 99 wt%), nickel(II) sulfate hexahydrate ($NiSO_4 \cdot 6H_2O$, 99 wt%), urea (99 wt%), sodium citrate dihydrate ($Na_3C_6H_5O_7 \cdot 2H_2O$, 99 wt%.), lead (II) bromide ($PbBr_2$, 99 wt%), cesium bromide (CsBr, 99 wt%), N, N-Dimethylmethanamide (DMF, 99 wt%), oleic acid (OA, 99 wt%), oleylamine (OAm, 98 wt%), toluene (99 wt%), ethyl acetate (EA, 99 wt%), and isopropanol (IPA, 70 wt% in H_2O) were purchase from Sigma-Aldrich.

1.3 Characterization

The morphology was recorded on the Zeiss Auriga scanning electron microscopy (SEM) and JEOL 2200FS transmission electron microscopy (TEM). The X-ray diffraction (XRD) patterns were collected on a Rigaku D max-3C diffractometer using Cu Kα radiation. X-ray photoelectron spectroscopy (XPS) was performed on an ESCALAB 250Xi spectrometer (Thermo Fisher Scientific). Peaks fitting of the high-resolution data was carried out by Thermo Avantage 5.992 surface chemical analysis software. UV-vis absorption spectra were recorded with a UV-vis-NIR spectrophotometer (Shimadzu UV-3600). The steady-state photoluminescence (ss-PL) spectra of the samples were measured on a fluorescence spectrophotometer (Horiba Scientific). Time-resolved photoluminescence (TR-PL) spectra were measured using a 2x Single-Photon Avalanche Diodes detector (PicoQuant Microtime 200). The electrochemical test was studied on a standard three-electrode configuration, with the samples coated on FTO substrate as the working electrode, platinum plate as the counter electrode, and Ag/AgCl electrode as the reference electrode. A solution of 0.01 M tetrabutylammonium hexafluorophosphate (TBAPF6) was used as the electrolyte. The anodic and cathodic photocurrent tests were recorded on a CHI 660D electrochemical station under the illumination of a 150 W Xe lamp (Lamphouse CX-05E, $\lambda > 420$ nm) at a potential of +0.3 V and -0.3 V vs. Ag/AgCl.

1.4 Catalytic test and product analysis

During the photocatalytic reduction, 5 mg as-synthesized catalysts powders were dispersed in 30 mL ethyl acetate and 460 μL isopropanol was added as a sacrificial agent. The mixture was carried out in a 100 mL sealed autoclave and then vacuumed and filled with purity CO_2 gas to reach a 0.2 kPa pressure at an ambient temperature (298 K). A 300 W Xenon lamp (Lamphouse CX-05E) coupled with a 420 nm cut-off filter (λ>420 nm) was used as the light source to simulate the solar light irradiation. The gaseous products were sampled by a gas-tight syringe and analyzed by a gas chromatograph (GC-2060, Shanghai Ruimin Instrument Co., Ltd.) equipped with a thermal conductivity detector (TCD) and a flame ionization detector (FID). High purity Argon (99.99%) was used as the carrier gas. To assess the stability of the catalysts, three consecutive runs of photocatalytic CO_2 reduction (6 h in each run) were conducted. Between each run, the reactor was vacuumed and refilled with CO_2.

2. Supporting figures

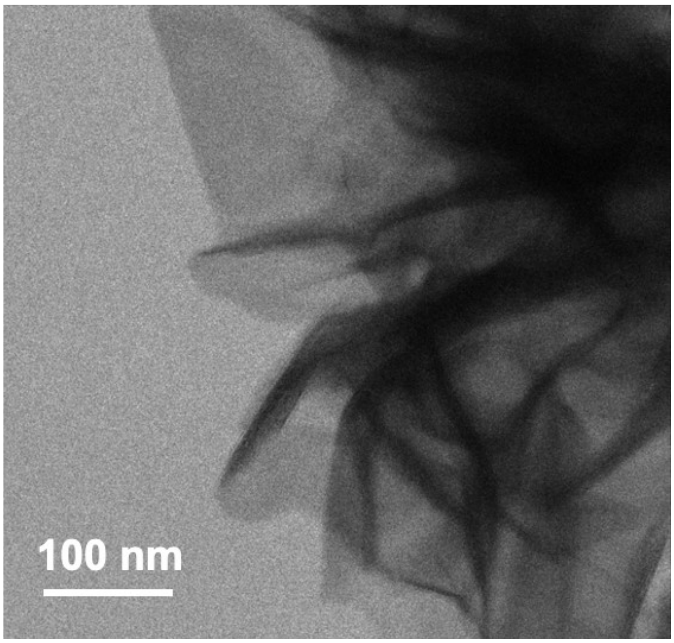

Figure S1. Characterization of TEM image of NiFe-LDH.

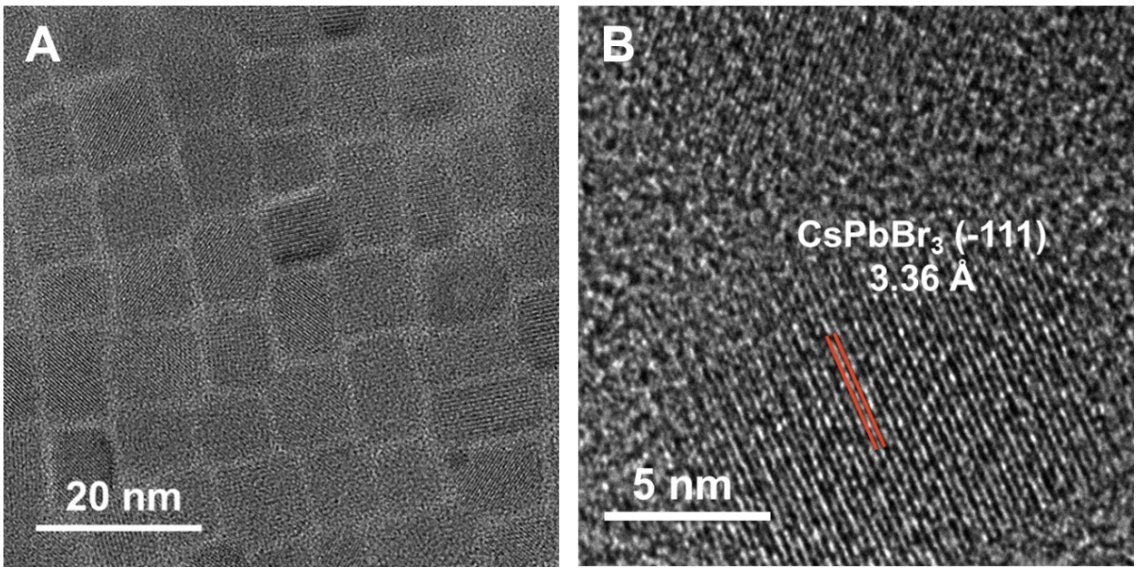

Figure S2. (A-B) TEM and HR-TEM images of $CsPbBr_3$ nanocrystals.

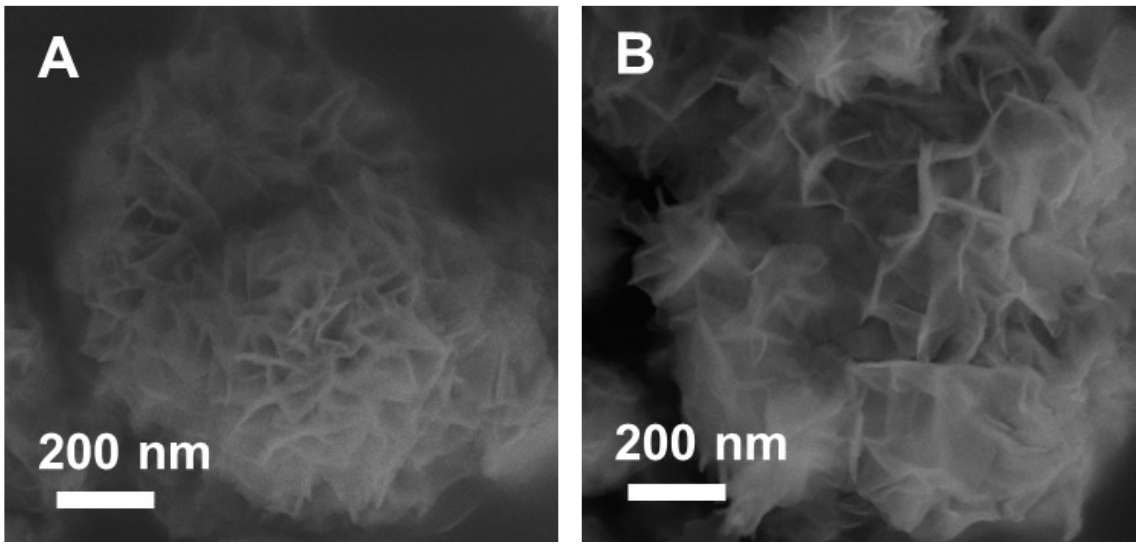

Figure S3. (A-B) SEM images CPB/NiFe-LDH-1 and CPB/NiFe-LDH-3 catalysts.

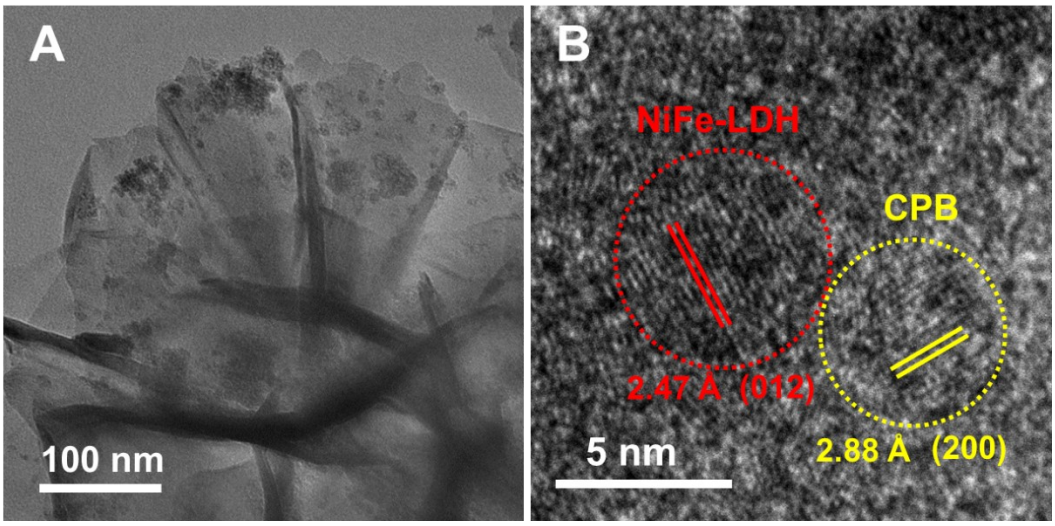

Figure S4. (A-B) TEM image and HR-TEM images of CPB/NiFe-LDH-2. The marked d-spacing of 2.88 Å and 2.47 Å can be indexed to the (200) plane of CPB and the (012) plane of NiFe-LDH, respectively.

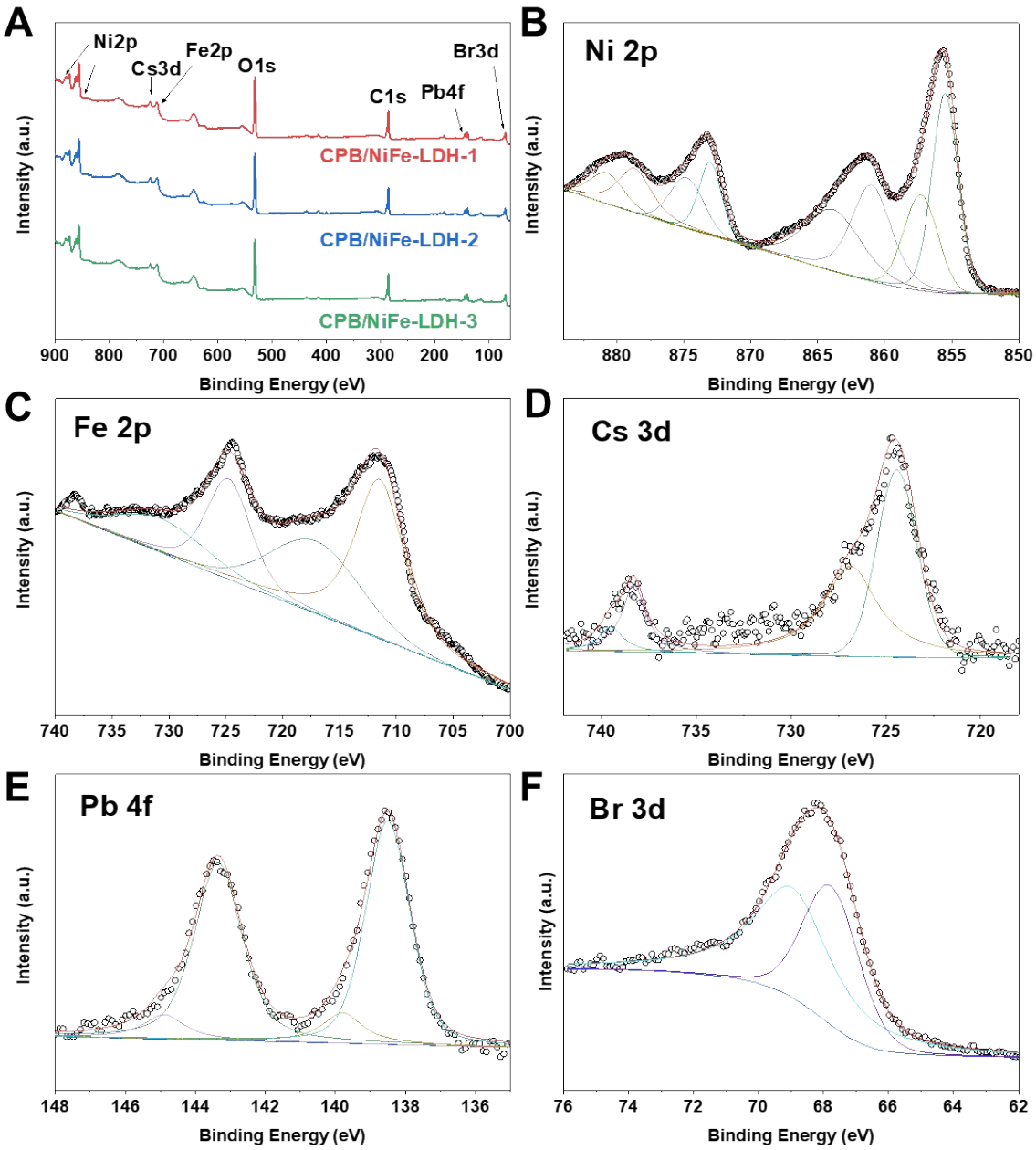

Figure S5. (A) XPS survey spectra of CPB/NiFe-LDH-1, CPB/NiFe-LDH-2 and CPB/NiFe-LDH-3. High-resolution XPS spectra of (B) Ni 2p, (C) Fe 2p, (D) Cs 3d, (E) Pb 4f, and (F) Br 3d.

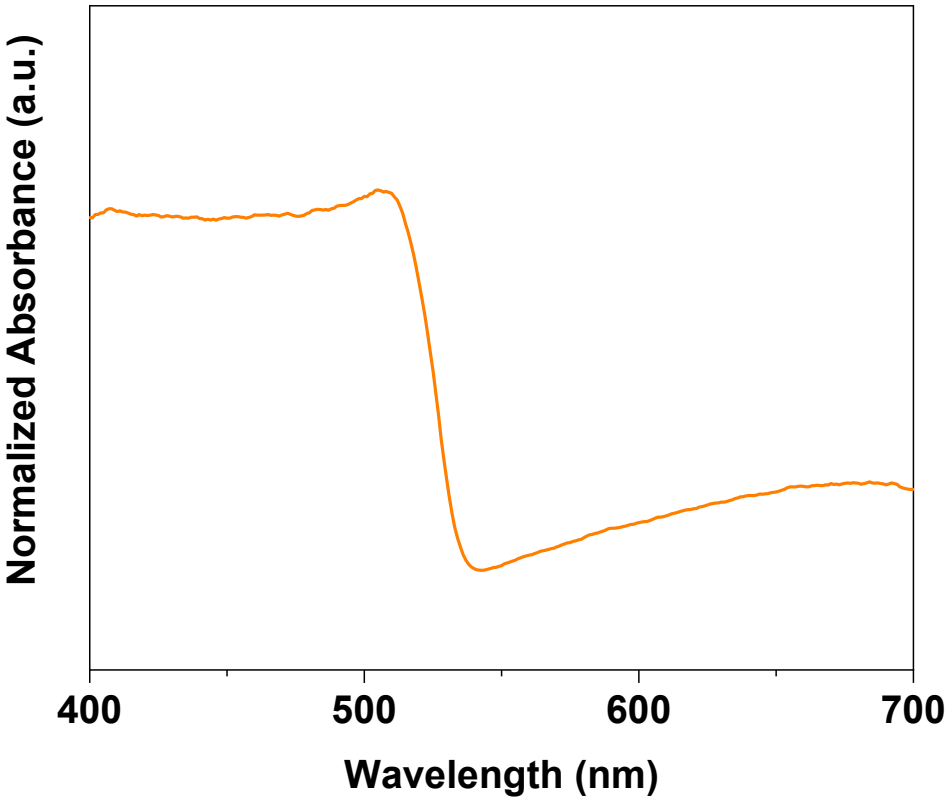

Figure S6. UV-vis absorption spectra of CPB.

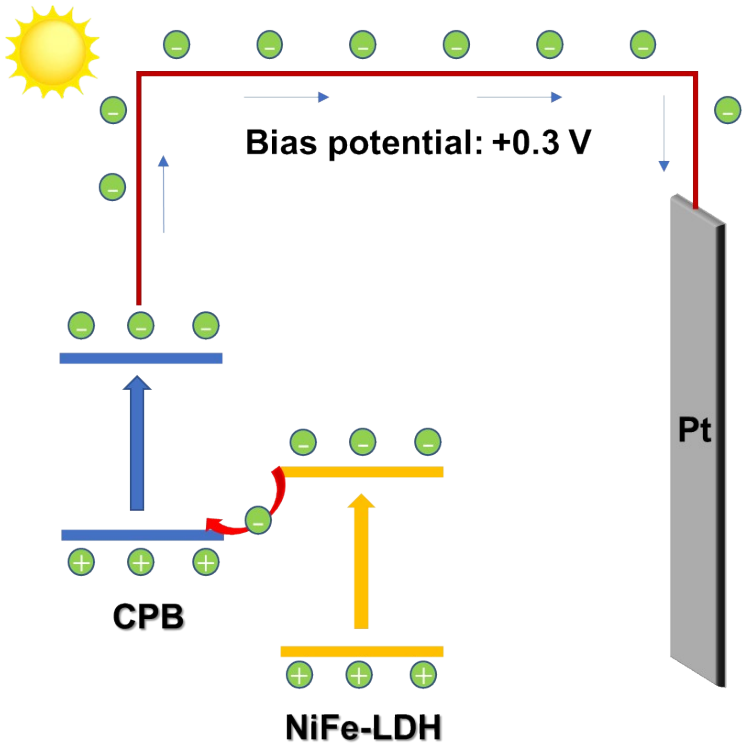

Figure S7. Scheme of the possible charge transfer direction in CPB/NiFe-LDH.

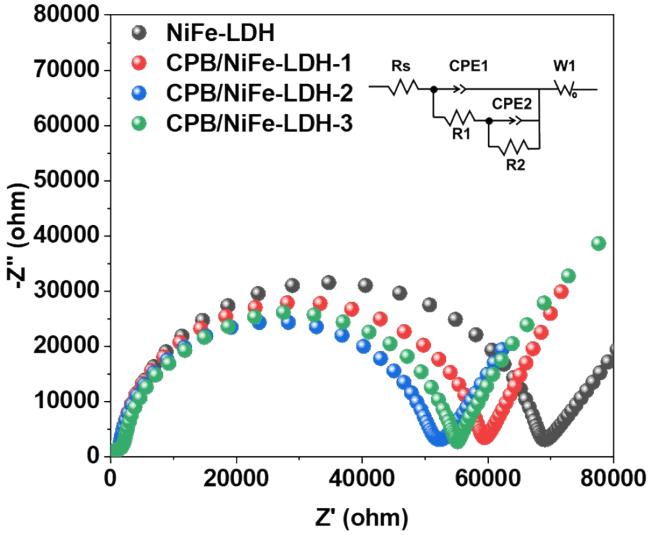

Figure S8. EIS plots of NiFe-LDH and CPB/NiFe-LDH-*x* (*x*=1, 2, 3).

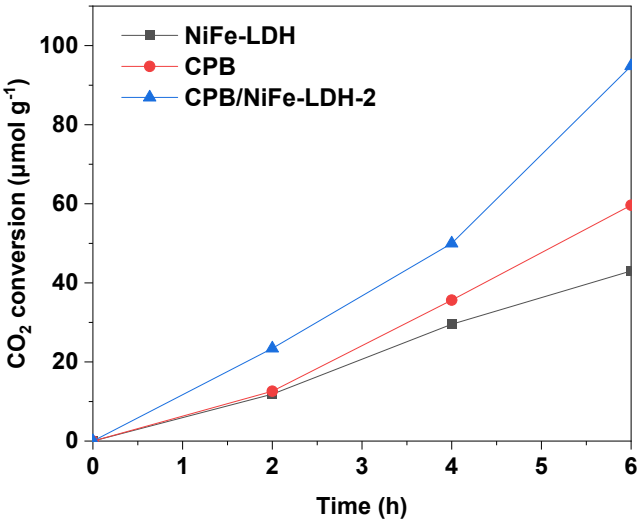

Figure S9. Time-online for photocatalytic CO_2 reduction of NiFe-LDH, CPB and CPB/NiFe-LDH-2.

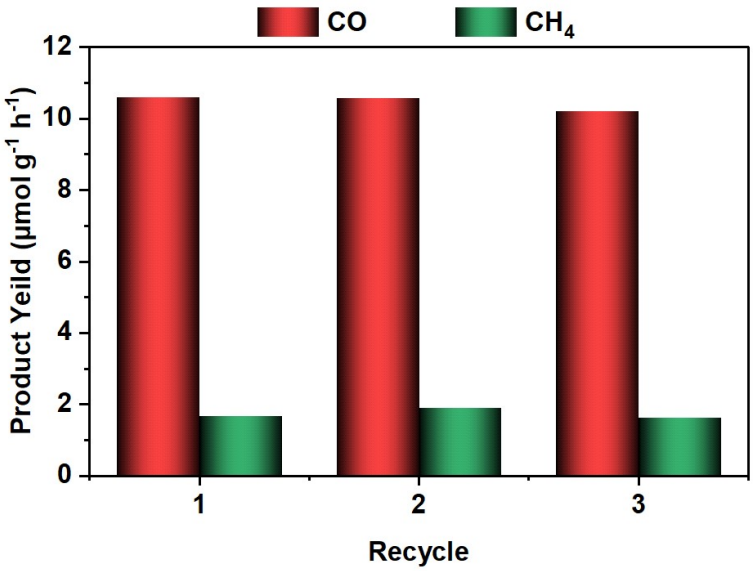

Figure S10. Recycling stability test of CPB/NiFe-LDH-2.

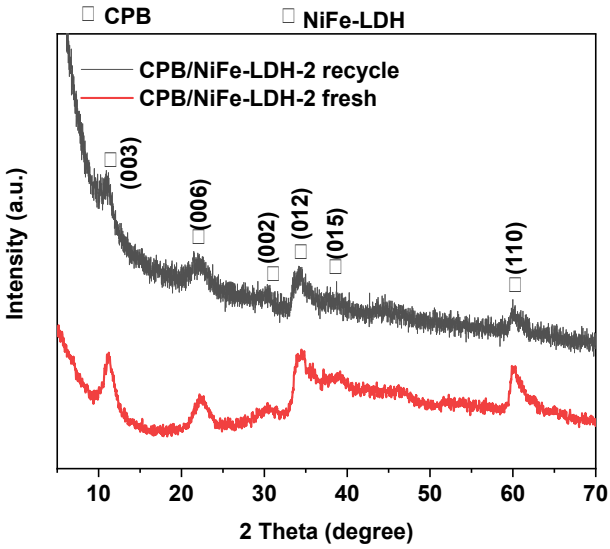

Figure S11. XRD pattern of CPB/NiFe-LDH-2 after 3 recycles and CPB/NiFe-LDH-2 fresh.

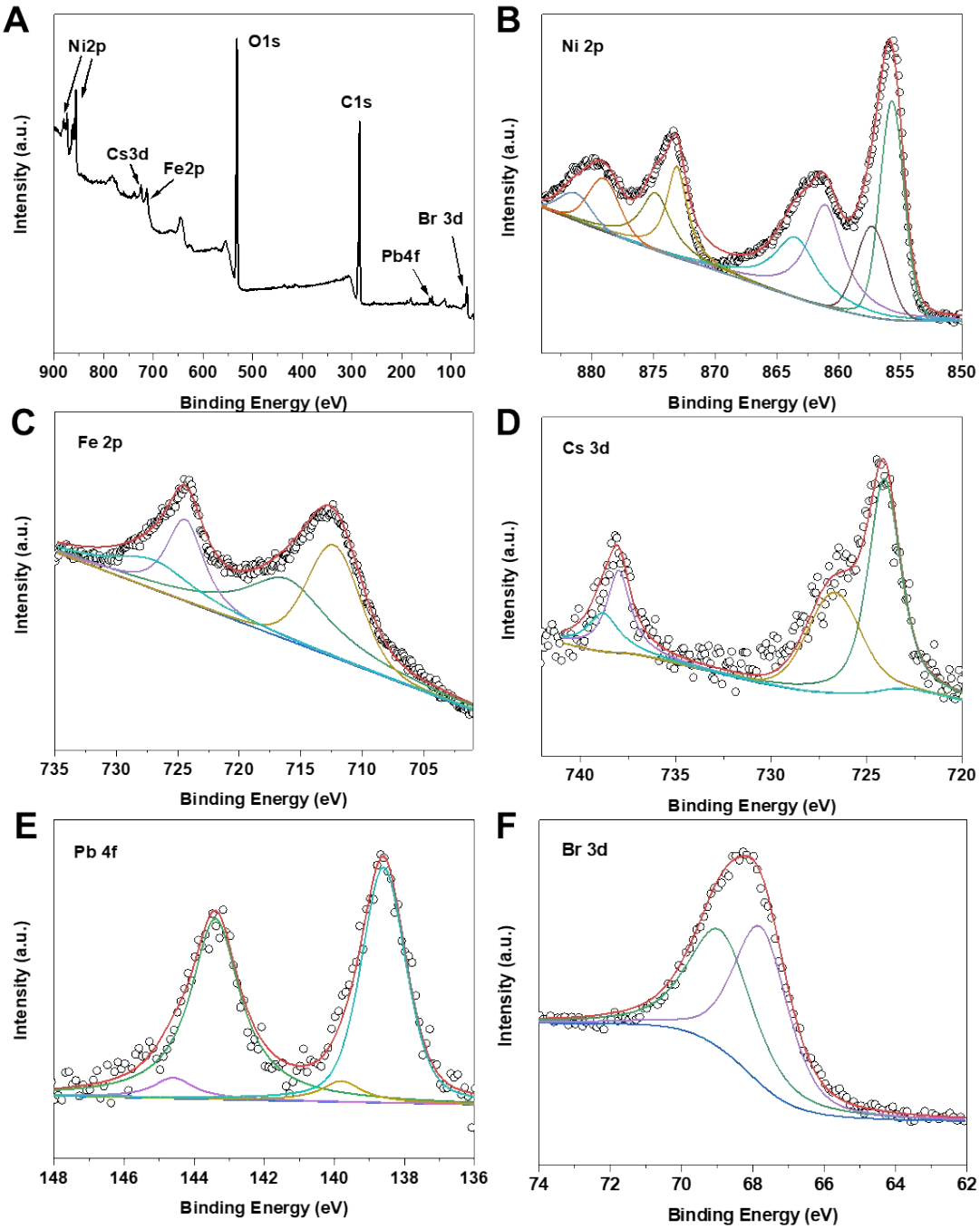

Figure S12. (A) XPS survey spectra of CPB/NiFe-LDH-2 and high-resolution XPS spectra of (B) Ni 2p, (C) Fe 2p, (D) Cs 3d, (E) Pb 4f, and (F) Br 3d after 3 cycles.

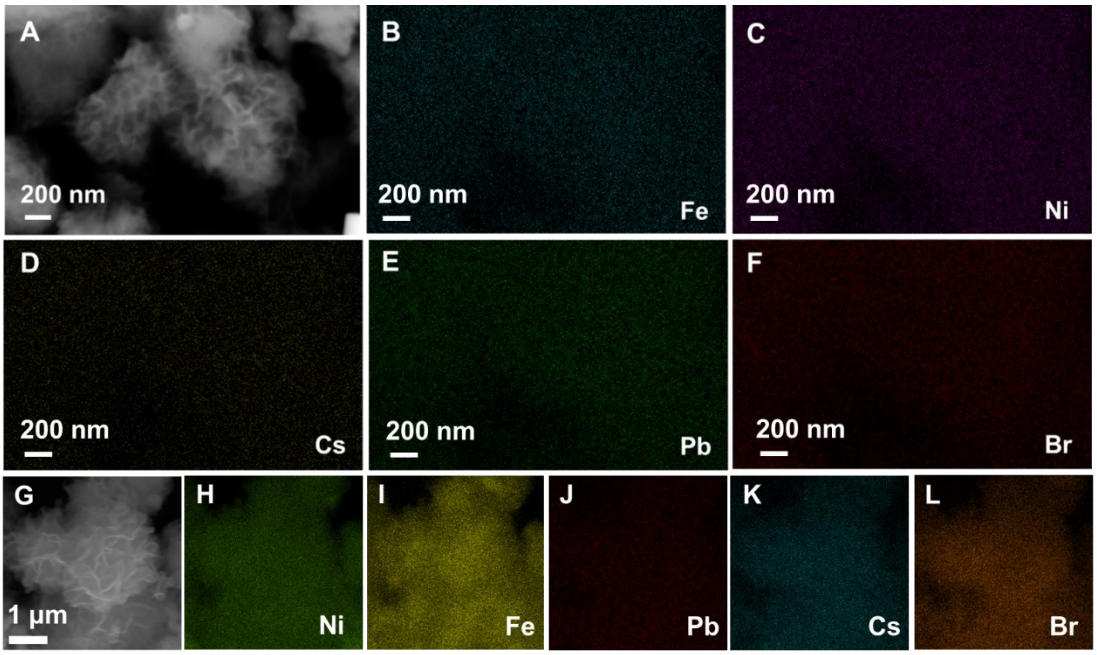

Figure S13. (A)SEM image, (B-F) EDS elements mapping images of CPB/NiFe-LDH-2 after 3 cycles, (G) SEM image, (H-L) EDS elements mapping images of CPB/NiFe-LDH-2 fresh.

3. Supporting Tables

Table S1. XPS atomic percentage analysis based on the survey spectra.

Sample	Atomic%		
	Ni	Br	Br/Ni
CPB/NiFe-LDH-1	5.91	2.71	0.46
CPB/NiFe-LDH-2	5.93	3.33	0.56
CPB/NiFe-LDH-3	5.92	3.65	0.62

Table S2. ICP analysis of CPB/NiFe-LDH-*x*.

Sample	wt%		
	Fe	Pb	Pb/Fe
CPB/NiFe-LDH-1	14.54	4.34	0.29
CPB/NiFe-LDH-2	15.69	5.42	0.35
CPB/NiFe-LDH-3	12.68	5.79	0.46

Table S3. Photogenerated charge lifetimes of NiFe-LDH, CPB/NiFe-LDH-*x*.

Sample	τ_1(ns)	τ_2(ns)	τ_3(ns)	τ_{ave}
NiFe-LDH	0.33	0.12	3.89	0.59
CPB/NiFe-LDH-1	0.34	0.10	4.75	1.55
CPB/NiFe-LDH-2	1.60	0.34	6.99	3.89
CPB/NiFe-LDH-3	0.60	0.13	6.83	3.41

Table S4. Comparison study of photocatalytic CO_2 reduction performance in this work and some latest reported perovskite-based photocatalysts towards CO_2 reduction.

Catalyst	CO_2 Conversion Rate (μmol h^{-1} g^{-1})	Selectivity			Reference
		CO	CH_4	H_2	
0.1-Pt/ex-LDH	2.64	> 99 %	-	-	Ref.[1]
20 wt% P25@CoAl-LDH	2.21	94 %	-	6 %	Ref. [2]
NiAl-LDH/CdS-2	12.45	96 %	4 %	-	Ref. [3]
5% GO-LDH	8.40	55 %	45 %	-	Ref. [4]
CPB/MS (1.0 wt%)	37.8	66 %	34 %	-	Ref. [5]
$CsPbBr_3$-GO NHSs	25.5	91.5 %	-	8.5 %	Ref. [6]
TiO_2/$CsPbBr_3$	6.72	95 %	-	5%	Ref. [7]
$CsPbBr_3$/GO	29.78	65 %	33 %	2 %	Ref. [8]
$CsPbBr_3$@ZIF-67	29.63	18 %	82 %	-	Ref. [9]
CPB/NiFe-LDH-2	39.58	83 %	17 %	-	This work

Table S5. Performance of photocatalysts towards CO_2 reduction.

Catalysts	AQY (%)
NiFe-LDH	0.38
CPB	0.35
CPB/ NiFe-LDH-1	0.42
CPB/ NiFe-LDH-2	0.70
CPB/ NiFe-LDH-3	0.47

The photocatalytic performance of pure Nife-LDH, CPB and CPB/Nife-LDH-*x* composites for CO_2 reduction were using a 300 W Xenon-arc lamp with a 420 nm cut-off filter (λ>420 nm) to simulate visible-light irradiation. For a typical test in photocatalytic CO_2 reduction, 5 mg photocatalyst was suspended in 30 mL ethyl acetate and 460 μL isopropanol. The obtained solution was vacuum-treated for 10 min. Then the suspension was filled with CO_2 for 10 min to reach the equilibrium of adsorption-desorption. The catalyst suspension was illuminated for 6 h. The average power intensity of the incident light was measured to be 1.5W by a photometer. The number of incident photos (N) is calculated by Equation 1 The gas chromatograph (GC-2010, SHIMADZU, Japan) was used to test the products in our test. The apparent quantum yield (AQY) at 420 nm wavelength was estimated via the following Equation 2:

$$N = \frac{E\lambda}{hc} = \frac{1.5 \times 6 \times 3600 \times 420 \times 10^{-9}}{6.626 \times 10^{-34} \times 3 \times 10^{8}} = 6.85 \times 10^{22} \quad \text{(Equation 1)}$$

$$AQY_{CO_2\ Reduction}(\%) = \frac{2 \times number\ of\ CO + 8 \times number\ of\ CH_4}{number\ of\ incident\ photons} \quad \text{(Equation 2)}$$

4. Reference

[1] J. Xu, X. Liu, Z. Zhou, L. Deng, L. Liu, M. Xu, Platinum Nanoparticles with Low Content and High Dispersion over Exfoliated Layered Double Hydroxide for Photocatalytic CO_2 Reduction, Energy Fuels, 35 (2021) 10820-10831.
[2] S. Kumar, M.A. Isaacs, R. Trofimovaite, L. Durndell, C.M.A. Parlett, R.E. Douthwaite, B. Coulson, M.C.R. Cockett, K. Wilson, A.F. Lee, P25@CoAl layered double hydroxide heterojunction nanocomposites for CO2 photocatalytic reduction, Appl. Catal. B ., 209 (2017) 394-404.
[3] X. Zhang, Y. Yang, L. Xiong, T. Wang, Z. Tang, P. Li, N. Yin, A. Sun, J. Shen, 3D dahlia-like NiAl-LDH/CdS heterosystem coordinating with 2D/2D interface for efficient and selective conversion of CO_2, Chin. Chem. Lett., (2021).
[4] K. Wang, C. Miao, Y. Liu, L. Cai, W. Jones, J. Fan, D. Li, J. Feng, Vacancy enriched ultrathin TiMgAl-layered double hydroxide/graphene oxides composites as highly efficient visible-light catalysts for CO_2 reduction, Appl. Catal. B, 270 (2020) 118878.
[5] X. Wang, J. He, L. Mao, X. Cai, C. Sun, M. Zhu, $CsPbBr_3$ perovskite nanocrystals anchoring on monolayer MoS_2 nanosheets for efficient photocatalytic CO_2 reduction, Chem. Eng. J., 416 (2021) 128077.
[6] Y.-H. Chen, J.-K. Ye, Y.-J. Chang, T.-W. Liu, Y.-H. Chuang, W.-R. Liu, S.-H. Liu, Y.-C. Pu, Mechanisms behind photocatalytic CO_2 reduction by $CsPbBr_3$ perovskite-graphene-based nanoheterostructures, Appl. Catal. B, 284 (2021) 119751.
[7] F. Xu, K. Meng, B. Cheng, S. Wang, J. Xu, J. Yu, Unique S-scheme heterojunctions in self-assembled TiO_2/$CsPbBr_3$ hybrids for CO_2 photoreduction, Nat. Commun., 11 (2020) 4613.
[8] Y.-F. Xu, M.-Z. Yang, B.-X. Chen, X.-D. Wang, H.-Y. Chen, D.-B. Kuang, C.-Y. Su, A $CsPbBr_3$ Perovskite Quantum Dot/Graphene Oxide Composite for Photocatalytic CO_2 Reduction, JACS, 139 (2017) 5660-5663.
[9] Z.-C. Kong, J.-F. Liao, Y.-J. Dong, Y.-F. Xu, H.-Y. Chen, D.-B. Kuang, C.-Y. Su, Core@Shell $CsPbBr_3$@Zeolitic Imidazolate Framework Nanocomposite for Efficient Photocatalytic CO_2 Reduction, ACS Energy Lett., 3 (2018) 2656-2662.